JSES International ■ (2020) 1–9

Contents lists available at ScienceDirect

JSES International

journal homepage: www.jsesinternational.org

Influence of reverse total shoulder arthroplasty baseplate design on torque and compression relationship

Miguel A. Diaz, MS [a], Jason E. Hsu, MD [b], Eric T. Ricchetti, MD [c], Grant E. Garrigues, MD [d], Sergio Gutierrez, PhD [a], Mark A. Frankle, MD [e,*]

[a] Foundation for Orthopaedic Research and Education, Tampa, FL, USA
[b] Department of Orthopaedics and Sports Medicine, University of Washington, Seattle, WA, USA
[c] Department of Orthopaedic Surgery, Cleveland Clinic Foundation, Cleveland, OH, USA
[d] Midwest Orthopaedics at Rush, Rush University Medical Center, Chicago, IL, USA
[e] Florida Orthopaedic Institute, Tampa, FL, USA

ARTICLE INFO

Keywords:
Baseplate design
RSA baseplate
baseplate micromotion
baseplate compression
stability

Level of Evidence: Basic Science Study: Biomechanics

Background: A linear relationship between baseplate insertion torque and compression force in reverse shoulder arthroplasty (RSA) baseplates with central screw design has been recently established. In this study, we evaluated 3 different baseplate designs and their influence on the torque-compression relationship.
Methods: Three different RSA baseplate designs were evaluated through biomechanical testing using a glenoid vault, bone surrogate model. A digital torque gauge was used to measure insertion torque applied to the baseplate, whereas compression data were collected continuously from a load cell. Additionally, 2 predictive models were developed to predict the compression forces of each baseplate design at varying levels of torque.
Results: A linear relationship was found between baseplate compression and insertion torque for all 3 baseplate designs. Both the monoblock and 2-piece locking designs achieved the goal torque of 6.8 Nm, whereas the 2-piece nonlocking design did not due to material strip-out. No significant difference in maximum compression was found between the monoblock and 2-piece locking designs. However, the 2-piece nonlocking design achieved significantly higher compression. Both predictive models were shown to adequately predict compressive forces at different torque inputs for the monoblock and 2-piece locking designs but not the 2-piece nonlocking design.
Conclusion: The torque-compression relationship of a central screw baseplate is significantly affected by baseplate design. A 2-piece nonlocking baseplate reaches higher compression levels and risks material strip-out at lower insertional torques compared with a monoblock and 2-piece locking design. This has implications both on component design and on surgeon tactile feedback during surgery.

The use of reverse shoulder arthroplasty (RSA) has risen dramatically in the past 2 decades, and indications for its use have expanded substantially.[5,19,42] Significant improvements in functional outcomes are evident in the published literature for a variety of indications.[26,29,33] Although the rates of reoperation and revision associated with RSA have decreased, implant-related complications are still significantly more common in RSA designs compared with anatomic shoulder arthroplasty designs.[2-6,28,31,32,35-39,42]

Glenoid baseplate loosening is one implant-related complication that can result from a number of potential factors including poor bone quality, inadequate initial biomechanical stability, and lack of bone ingrowth onto the prosthesis.[7,16-18,27,28] The prosthetic design of a glenoid baseplate can affect both initial fixation and long-term survivorship—several biomechanical studies have explored options to improve initial fixation and minimize micromotion[16-18,20,24] with use of various types and configurations of peripheral screws,[16,21,22,30] various baseplate positions and orientations,[1,30,40,41] and multiple baseplate designs.[8,23,36,39,40]

The initial fixation strength of a glenoid baseplate construct, as well as tactile feedback to the surgeon, can be affected by both the applied torque during insertion of a central-screw baseplate and the resultant axial compressive forces on the glenoid bone.[13] The relationship between torque and compression can theoretically be affected by a number of baseplate design features including modularity (1- vs. 2-piece design), locking and nonlocking features

Institutional review board approval was not required for this basic science study.

* Corresponding author: Mark A. Frankle, MD, Florida Orthopaedic Institute 13020 N Telecom Pkwy, Tampa, FL 33637, USA
E-mail address: mfrankle@floridaortho.com (M.A. Frankle).

https://doi.org/10.1016/j.jseint.2020.02.004

of a central screw, shape of the baseplate, length and diameter of the central screw, and component surface roughness.

The relationship between insertion torque and baseplate compression in a central screw baseplate design has been recently evaluated.[13] However, data quantifying the relationship between these clinically relevant variables of torque and compression with different baseplate constructs is currently lacking in the literature. Therefore, the primary objective of this study was to investigate the compressive forces generated by varying levels of torque using 3 different baseplate designs: an established monoblock central screw design, a 2-piece baseplate with a locking central screw, and a 2-piece baseplate with a nonlocking central screw. Our hypothesis was that a monoblock and 2-piece locking baseplate would achieve similar compressive forces at all levels of torque, whereas a 2-piece nonlocking baseplate would achieve higher levels of compression at similar torque levels. A secondary objective was to create a finite element analysis (FEA) model and mathematical model, capable of predicting compressive forces for a given torque and comparing this to observed mechanical testing. We hypothesized that the relationship between applied torque and compression will be linear and that the output of the FEA model will be comparable to mechanical testing and mathematical modeling for each baseplate design.

Materials and methods

Baseplate designs

Baseplate designs used for this study included the following: (1) a monoblock design printed by 3-dimensional (3D) direct metal laser sintering and made out of 316L stainless steel with the same nominal dimensions as a commercially available implant (RSP; DJO Global, Austin, TX, USA), including a 26-mm-diameter baseplate and a 6.5-mm central cancellous bone screw measuring 30 mm in length; (2) a custom-designed 2-piece locking 3D direct metal laser sintering printed baseplate patterned off of the commercially available monoblock design that included a baseplate portion with a central cavity and internal threads to accept a separate 6.5-mm central cancellous screw with external threads on the head of the screw; and (3) a custom-designed 2-piece nonlocking 3D direct metal laser sintering printed baseplate patterned off of the commercially available monoblock design that included a baseplate portion with a smooth central cavity that accepts a separate 6.5-mm central cancellous screw with a smooth screw head (Fig. 1).

Bone surrogate (30 PCF)

A previously published testing model was used to create bone surrogates with cortical and cancellous features.[13] Briefly, solid rigid polyurethane foam blocks (30 PCF, Model 1522-04; Pacific Research Laboratories, Vashon, WA, USA) were cut into 6 cubes (50× 50×40-mm) using a vertical bandsaw. The centers of each cube were marked and, in accordance with manufacturer recommendations, a 2.5-mm pilot hole was created for the 30 PCF cubes using a drill press. For all tested baseplate designs, the center holes were prepared to 30 mm using the manufacturer's threaded tap, where 2 passes were done to ensure threads in the foam blocks were clean and free of debris. To simulate the contact between the undersurface of the baseplate and the surface of the glenoid face, epoxy resin sheets (Model 3401-03; Pacific Research Laboratories) (density 102 PCF or 1.65 g/cm^3) were used. The stock sheets (130×180×2-mm) were cut into squares (50×50×2-mm), and a central hole was created to match that of the foam blocks. The sheets were then resurfaced with the manufacturer's reaming guide such that the baseplate would sit flush. To maintain consistency throughout testing, each foam block had its own unique epoxy resin square and was only used once per test.

Biomechanical testing

A total of 18 bone surrogate foam blocks (n=6 per baseplate design) were prepared as described above to simulate the glenoid bone vault.[13] A custom-designed fixture that allowed each foam block to be secured to a 6–degree-of-freedom loadcell (MC3A-1000 lb, 0.2% accuracy; AMTI Transducers, Watertown, MA, USA) was

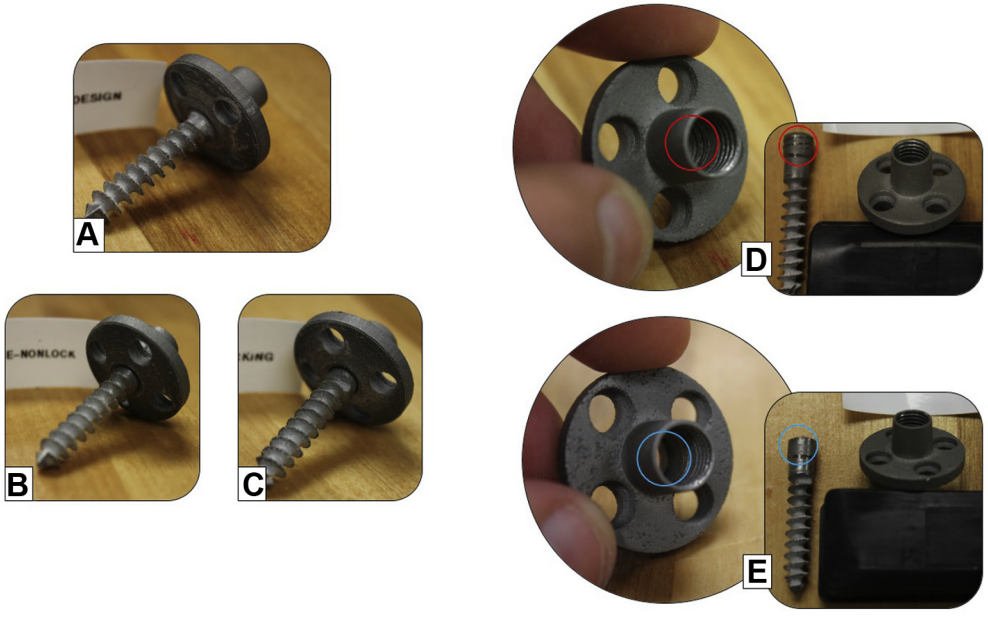

Figure 1 Illustration of 3D direct metal laser sintering baseplate designs: (**A**) monoblock, (**B**) 2-piece nonlocking, (**C**) 2-piece locking. (**D**) Side-by-side view of the central screw and baseplate design for the 2-piece locking design, where the proximal threaded end of the central screw locks into the internal threads of the baseplate, as highlighted by the red circles. (**E**) Side-by-side view of the 2-piece nonlocking design, where the blue circles highlight the smooth proximal end of the central screw and no locking threads in the baseplate.

developed, as previously described,[13] and used to explore the relationship between torque and compression (Fig. 2). Insertion torque of a baseplate with central screw has been measured intraoperatively to be at least 6.8 Nm (60 in.lbf) during baseplate fixation into human glenoid bone.[13,20] A digital torque gauge (HTGS-85, 0.5% accuracy; IMADA, Northbrook, IL, USA) was used to apply incremental amounts of torque to each baseplate (range: 0-6.8 Nm [0-60 in.lbf], by increments of 1.1 Nm [10 in.lbf]) when inserting the implants into the foam blocks. Compression data from the load cell was continuously collected at a rate of 60 Hz using a custom program in LabView (National Instruments, Austin, TX, USA). The compression force afforded by each baseplate for each bone surrogate was defined as the average of the plateau region on the force-time curve for each torque level. Material deformation or "stripping" was defined as a reduction in torque followed by a decrease in compression readout. In circumstances where a specified torque level was not attainable, the maximum compression force and respective torque value before stripping were reported. The primary endpoint was assessing the relationship between insertion torque and compression across baseplate designs.

Finite element analysis

FEA was performed using the SolidWorks Simulation package in SolidWorks (SolidWorks 2018, Dessault Systèmes, Cedex France). The same 3 baseplate designs used in the biomechanical testing were modeled with the baseplate, epoxy sheet, top plate, Sawbones block, and bottom plate (Fig. 3). Material properties are summarized in Table I and boundary conditions are summarized in Table II. The models used a solid curvature-based mesh with a total of 49,303 nodes and 32,262 elements for the monoblock baseplate model, 46,680 nodes, and 29,167 elements for the 2-piece locked baseplate model and 52,651 nodes and 32,254 elements for the 2-piece non-locked baseplate model. The simulation used a linear elastic isotropic Direct Sparse solver. The simulation applied a linearly ramped torque up to 6.8 Nm (60 in.lbf) on the top of the baseplates mimicking the force applied by a screwdriver. Data were plotted as compression vs. torque and the relationship was analyzed.

Mathematical modeling

The calculation of screw compression was performed using equations from *Machinery's Handbook*, 29th edition[33] (Fig. 4). The equation was used to calculate compression at 1.13 Nm (10 in.lbf) increments, to 6.8 Nm (60 in.lbf) (Fig. 5). Data were plotted as compression vs. torque, and the relationship was analyzed.

Statistical analysis

The relationship between insertion torque and compression for each baseplate design was plotted and analyzed for biomechanical testing. Data are presented as mean ± standard deviation. Test for linearity and Pearson correlation (PC) were conducted to evaluate potential correlations between baseplate compression, insertion torque, and baseplate design. A Kruskal-Wallis test was used to evaluate the compressive force at each torque input across baseplate designs. Bonferroni correction was used for post hoc analysis. Level of significance was set at $P \leq .05$.

To test how well the FEA and mathematical models predicted compression of each baseplate design at a given torque, *t* statistics were used to compare the slope of linear regression models of the FEA and mathematical model to that of the biomechanical model. Because multiple *t* statistics were performed to compare the slope of linear regressions, alpha (α=0.05) was adjusted with Bonferroni correction to reduce Type I error while generating the new alpha ($\alpha_N = 0.05/6 = 0.0083$). All statistical operations were performed using SPSS, version 22 (IBM, Armonk, NY, USA).

Results

Biomechanical testing

A linear regression analysis for each baseplate design presented evidence of a strong positive correlation between torque input and compression (monoblock: $R^2 = 0.996$, $P < .001$, PC = 0.997; 2-piece locking: $R^2 = 0.995$, $P < .001$, PC = 0.997; 2-piece nonlocking: $R^2 = 0.999$, $P < .001$, PC = 0.999). Samples tested with the Monoblock

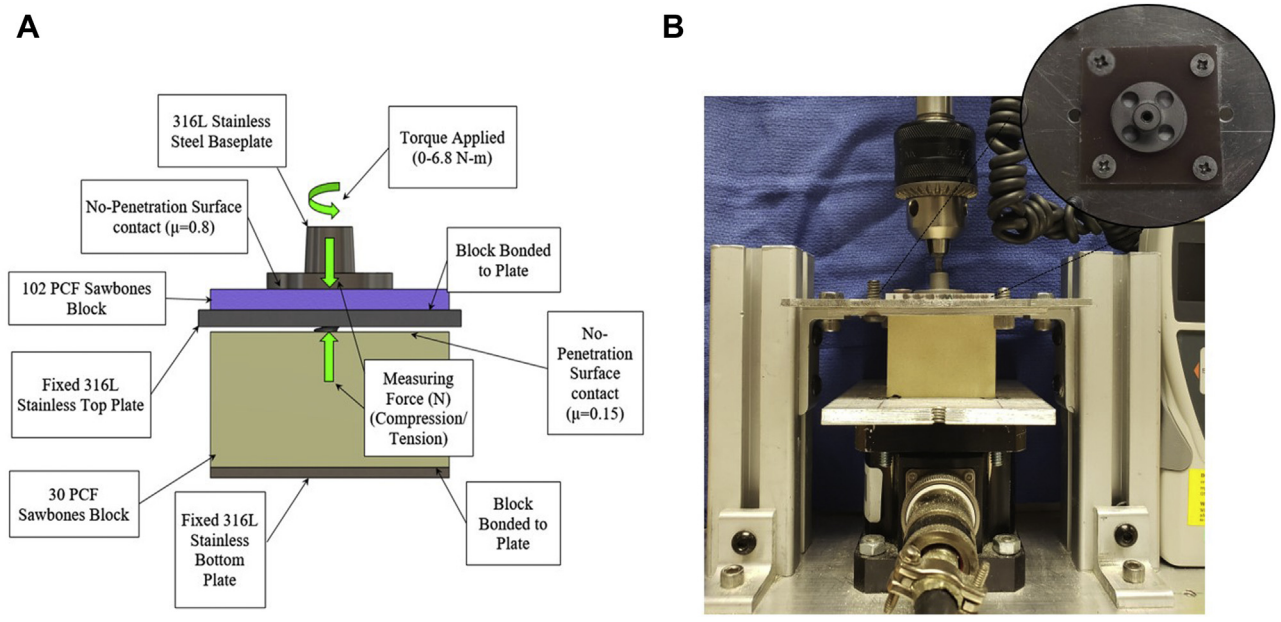

Figure 2 (**A**) Detailed illustration of biomechanical setup; (**B**) actual experimental setup with a close-up of the top view. Each tested foam block was fixed to the load cell, which continuously collected data. Baseplates fit flush on the epoxy sheet, which was fixed to a rigid platform at 5 mm. Torque was applied with a digital torque gauge (maximum 6.8 Nm [60 in.lbf]).

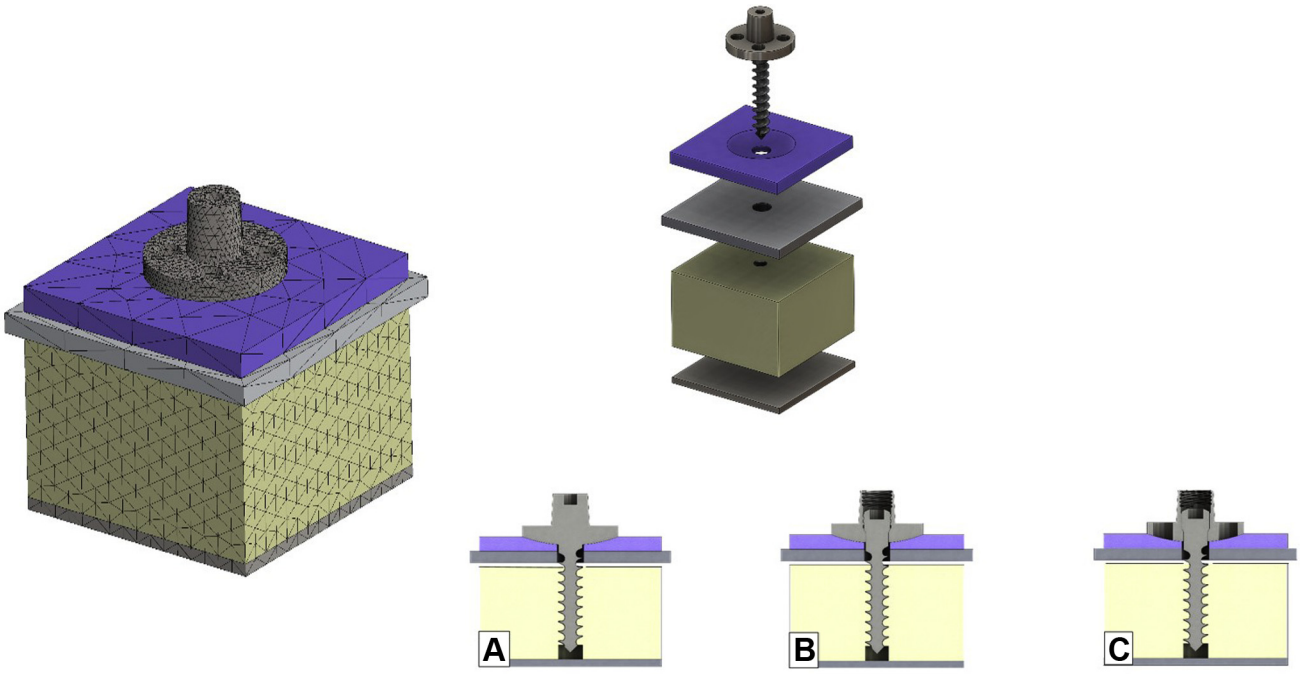

Figure 3 FEA mesh model used to run predictive analysis. This model closely replicated the biomechanical testing model as illustrated by the cross-sectional images of computer-aided design used for FEA: (**A**) monoblock baseplate design, (**B**) 2-piece locking baseplate design; and (**C**) 2-piece nonlocking design. *FEA*, finite element analysis.

and 2-piece locking designs all achieved the goal torque of 6.8 Nm. Maximum compression for the monoblock and 2-piece locking designs were 785.67 ± 71.2 N and 786.6 ± 82.8 N, respectively. Because of foam block stripping, none of the samples tested with the 2-piece nonlocking baseplate design achieved the goal torque of 6.8 Nm. However, maximum compression of 888.6 ± 26.4 N was achieved at 4.5 Nm (Fig. 6).

From the independent samples Kruskal-Wallis Test, compression between baseplate designs were found to be significantly different at torque levels 1.13, 2.26, 3.39, and 4.52 Nm ($P = .003$, $P = .003$, $P = .003$, and $P = .007$, respectively). On post hoc analysis, the 2-piece nonlocking design attained significantly higher compression than the monoblock design at torque levels of 1.13, 2.26, 3.39, and 4.52 Nm ($P = .005$, $P = .007$, $P = .004$, and $P = .014$, respectively). Similarly, the 2-piece nonlocking design attained significantly higher compression than the 2-piece locking design at those same torque levels ($P = .021$, $P = .015$, $P = .028$, and $P = .019$, respectively). On post hoc analysis, no significant differences were detected between the monoblock and 2-piece locking designs for the compression attained at any of the torque levels (Fig. 6).

Biomechanical testing vs. FEA and mathematical modeling

Monoblock baseplate design

A linear regression analysis for the FEA and mathematical models (Fig. 7A) presented evidence of a strong positive correlation between torque input and compression (FEA: $R^2 = 0.984$, $P < .001$, PC = 0.992; Mathematical: $R^2 = 0.999$, $P < .001$, PC = 0.999).

Although the lower range of the FEA model predicted lower compression at low torque inputs, no significant difference was found when comparing the slope of the biomechanical model's linear regression to the linear regression of the FEA model (121.36 vs. 129.95 N/Nm; $P = .371$). Similarly, no significant difference was found when comparing the slope of the biomechanical model's linear regression to the linear regression of the mathematical model (121.36 vs. 122.33 N/Nm; $P = .809$).

Two-piece locking baseplate design

A linear regression analysis for the FEA and mathematical models (Fig. 7B) presented evidence of a strong positive correlation between torque input and compression (FEA: $R^2 = 0.994$, $P < .001$, PC = 0.997; mathematical: $R^2 = 0.999$, $P < .001$, PC = 0.999)

Table I
Material properties used to define our system for FEA

Parts	Material	Mass density, kg/m^3	Poisson'ratio	Elastic modulus, N/m^2	Shear modulus, N/m^2	Tensile strength, N/m^2	Compressive strength, N/m^2
Monoblock baseplate	316L stainless steel	8027	0.27	1.85E+11	8.20E+10	6.40E+08	3.10E+08
Two-piece baseplate	316L stainless steel	8027	0.27	1.85E+11	8.20E+10	6.40E+09	3.10E+08
Two-piece screw (locked)	316L stainless steel	8027	0.27	1.85E+11	8.20E+10	1.10E+09	3.10E+08
Two-piece screw (nonlocked)	316L stainless steel	8027	0.27	1.85E+11	8.20E+10	1.10E+09	3.10E+08
Sawbone block 102 PCF	Short fiber-filled epoxy	1640	0.35	1.60E+10	2.00E+09	1.06E+08	1.57E+08
Top metal plate	6061-T6 aluminum	2700	0.33	6.90E+10	2.60E+10	3.10E+08	2.80E+08
Sawbone block 30 PCF	Solid rigid polyurethane foam	480	0.3	5.95E+08	8.70E+07	1.20E+07	1.80E+07
Sawbone block SO PCF	Solid rigid polyurethane foam	800	0.3	1.47E+09	1.78E+08	2.70E+07	4.80E+07
Bottom metal plate	6061-T6 aluminum	2700	0.33	6.90E+10	2.60E+10	3.10E+08	2.80E+08

FEA, finite element analysis.

Table II
Boundary conditions used for FEA

Boundary conditions	Monoblock baseplate	Two-piece baseplate	Two-piece screw (locked)	Two-piece screw (nonlocked)	Sawbone block 102 PCF	Top metal plate	Sawbone block 30 PCF	Sawbone block 50 PCF	Bottom metal plate
Monoblock baseplate	Linear torque up to 6.8 Nm	N/A	N/A	N/A	No penetration friction factor = 0.8	N/A	N/A	N/A	N/A
Two-piece baseplate	N/A	Linear torque up to 6.8 Nm	No penetration friction factor = 0.3	No penetration friction factor = 0.3	No penetration friction factor = 0.8	N/A	N/A	N/A	N/A
Two-piece screw (locked)	N/A	No penetration friction factor = 0.3	N/A	N/A	N/A	N/A	No penetration friction factor = 0.1	No penetration friction factor = 0.1	N/A
Two-piece screw (nonlocked)	N/A	No penetration friction factor = 0.3	N/A	N/A	N/A	N/A	No penetration friction factor = 0.1	No penetration friction factor = 0.1	N/A
Sawbone block 102 PCF	No penetration friction factor = 0.8	No penetration friction factor = 0.8	N/A	N/A	N/A	Bonded	N/A	N/A	N/A
Top metal plate	N/A	N/A	N/A	N/A	Bonded	Fixed	N/A	N/A	N/A
Sawbone block 30 PCF	No penetration friction factor = 0.1	N/A	No penetration friction factor = 0.1	No penetration friction factor = 0.1	N/A	N/A	N/A	N/A	Bonded
Sawbone block 50 PCF	No penetration friction factor = 0.1	N/A	No penetration friction factor = 0.1	No penetration friction factor = 0.1	N/A	N/A	N/A	N/A	Bonded
Bottom metal plate	N/A	N/A	N/A	N/A	N/A	N/A	Bonded	Bonded	Fixed

FEA, finite element analysis.

No significant difference was found when comparing the slope of the biomechanical model linear regression to the linear regression of the FEA model (122.64 vs. 103.71 N/Nm; $P = .0129$). Similarly, no significant difference was found when comparing the slope of the biomechanical model's linear regression to the linear regression of the mathematical model (122.64 vs. 122.33 N/Nm; $P = .946$).

Two-piece nonlocking baseplate design

A linear regression analysis for the FEA and mathematical models (Fig. 7C) presented evidence of a strong positive correlation between torque input and compression (FEA: $R^2 = 0.997$, $P < .001$, PC = 0.998; mathematical: $R^2 = 0.999$, $P < .001$, PC = 0.999)

The slope of the biomechanical model linear regression was significantly larger than the slope of the linear regression for the FEA model (184.04 vs. 124.2 N/Nm; $P < .0083$). However, the slope of the biomechanical model linear regression was significantly lower when compared to the slope of the linear regression of the mathematical model (184.04 vs. 222.44 N/Nm; $P < .0083$).

Overall, both predictive models concluded that the 2-piece nonlocking design achieves higher compressive forces at lower torque ranges, whereas the monoblock and 2-piece locking designs behaved similarly (Fig. 8).

Discussion

The optimal baseplate design in RSA for both initial fixation and implant longevity continues to be investigated. The glenoid baseplate may use a central peg or screw fixation to attach the implant to the bone. With a central screw, the screw turns and the rotational force is then transferred into linear motion. As the head of the screw advances to the bone, compression develops between the screw head (or underlying baseplate) and the surface of the bone. There is a commensurate increase in torsional resistance as compression increases. As compression increases, stability at the implant-bone interface also increases.[9,14,34] The surgeon's tactile feedback of insertional torque during implantation of a central screw baseplate is thus used as a proxy for both implant compression and initial construct stability. The relationship between torque and compression has been previously investigated in a particular monoblock RSA baseplate design.[13] However, the effect of different central screw baseplate designs on the relationship between the insertional torque and the resultant compressive forces is not well-characterized. Therefore, the purpose of this study was to investigate the compressive forces generated by varying levels of torque using 3 different baseplate designs: an established monoblock central screw design, a 2-piece baseplate with a locking central screw, and a 2-piece baseplate with a nonlocking central screw.

The monoblock design used in this study has a strong clinical track record and has the theoretical advantage of eliminating a modular interface that may pose a risk for loosening or breakage.[10,11,25] However, the ability to simultaneously control baseplate rotation (and thus the position of peripheral screws) and insertional torque is limited. In some cases, this may affect the surgeon's decision on peripheral screw locations and also may limit the surgeon's ability to address asymmetrical glenoid defects if metal augmentation of bone loss is desired. Examples of current commercially available 2-piece baseplate designs are the Biomet (Warsaw, IN, USA) Comprehensive Reverse (nonlocked design), Stryker (Kalamazoo, MI, USA) ReUnion RSA (locked design), and the Wright Medical (Memphis, TN, USA) Aequalis Perform Reversed Glenoid (locked and nonlocked design), which all have a 6.5-mm central screw. Modular 2-piece designs allow for independent control of baseplate rotation and insertional torque, but the effect on torque-compression relationships is unknown. This

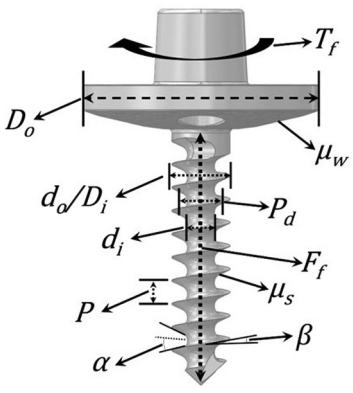

F_f	=	Compression/tension in screw
T_f	=	Torque applied to screw
d_o	=	Major diameter of screw
r	=	Radius of d_o
d_i	=	Minor diameter of screw
D_o	=	Outer diameter of bearing surface
D_i	=	Inner diameter of bearing surface
P	=	Pitch of threads
P_d	=	Pitch diameter of threads (r/2 + r)
μ_s	=	Coefficient of friction on threads
μ_w	=	Coefficient of friction on bearing surfaces
α	=	Thread half angle
β	=	Thread lead angle

Figure 4 Illustration of all the factors associated with the glenoid baseplate that are related to compression given a known torque input.

study demonstrates that higher compressive loads are obtained with lower insertional torque using a nonlocked 2-piece design compared to a monoblock design and a locking 2-piece design. The 2-piece mechanism described in this study provides a compression locking mechanism. The design provides increasing levels of compression as the screw head threads engage into the baseplate threads and then become a locked construct when the threads are fully seated into the baseplate. At this point, the baseplate functionally becomes a 1-piece (monoblock) baseplate with the ability to add more compression by rotating the whole construct. A nonlocking design allows for independent rotation of the central screw relative to the baseplate—allowing for more compression of the baseplate against bone by maximizing the engagement of the screw threads without coupling this to the frictional forces between the backside of the baseplate and the glenoid bone.

Potential failure mechanisms during insertion of a central screw baseplate include stripping of the central screw, breakage of the central screw, and excessive load or torque leading to bony fracture.[2-5,26,37] A previous study has demonstrated the potential for material strip-out with higher insertional torques in lower-density bone.[13] In our study, it was demonstrated that baseplate design features also affect the potential for material strip-out, specifically that the insertional torque required for screw strip-out is lower in a nonlocking 2-piece design than either the locking 2-piece design or the monoblock design. With a locking screw or monoblock design, the insertional torque is transferred both to the screw threads engaging into the bone and the friction interface between the backside of the baseplate and the glenoid bone. Because the torque on the central screw in a nonlocking design is not coupled to the baseplate, the baseplate-bone friction interface does not play as

$$F_f = 1000 \times \frac{T_f}{\left(\frac{1}{2d_o}\left(\frac{P}{\pi} + \mu_s P_d \sec\left(\tan^{-1}\left(\tan\alpha\cos\beta\right)\right) + \left(\mu_w \times \frac{2}{3}\left(\frac{D_o^3 - D_i^3}{D_o^2 - D_i^2}\right)\right)\right)\right) \times d_o}$$

Parameters	Monoblock	Two-Piece Locked	Two-Piece Non-Locked
T_f (N-m)	0 - 6.8	0 - 6.8	0 - 6.8
d_o (mm)	6.5	6.5	6.5
r (mm)	3.25	3.25	3.25
d_i (mm)	3	3	3
D_o (mm)	26.3	26.3	7.5
D_i (mm)	6.5	6.5	6.5
P (mm)	2.8	2.8	2.8
P_d (mm)	4.88	4.88	4.88
μ_s	0.15	0.15	0.15
μ_w	0.8	0.8	0.3
α (°)	22.5	22.5	22.5
β (°)	12	12	12

Figure 5 Mathematical equation that takes into account the above glenoid baseplate factors to output compressive force in newtons.

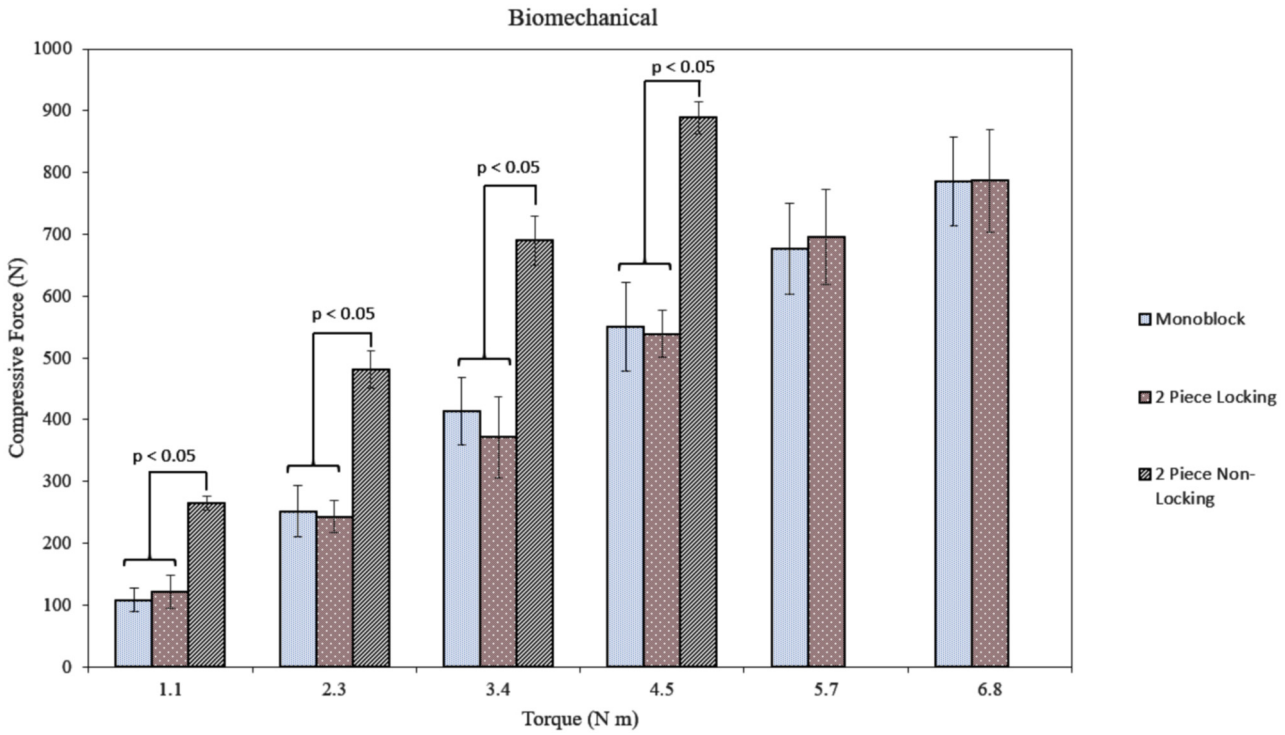

Figure 6 Means and standard deviations of measured compressive forces at increasing levels of torque for all 3 baseplate designs in the biomechanical testing model.

great a role, and the majority of the torque is transferred to the screw threads engaging in the bone. This has implications on the feedback to the surgeon during insertion of different baseplate designs—for a nonlocking central screw baseplate, the surgeon will want to consider stopping at a lower insertion torque given that the screw could strip out, particularly in lower-density bone. Surgeons must also take into consideration the additional interface between the central screw and baseplate in the nonlocking design—while allowing for additional compression with less torque, this interface may affect the ability of the overall construct to resist shear forces. However, these results should be interpreted with caution as other implant designs and manufacturers may rely on different mechanisms to achieve stability and fixation.

Computational modeling of orthopedic implants has allowed for efficient development and evaluation of different designs.[12,15] However, validation of these models with biomechanical data is necessary to ensure confidence in decisions related to its clinical application.[14] The FEA and mathematical models used in the current study were adequate in predicting compressive forces achieved at different torque inputs for 2 of the 3 baseplate designs tested. Both the FEA and mathematical models generated results similar to the biomechanical testing results at all torque levels for the monoblock and 2-piece locking designs. The mathematical model tended to overestimate the compressive forces, whereas the FEA tended to underestimate the forces. Despite these differences, the FEA and mathematical models still demonstrated higher torque-compression relationships with the 2-piece non-locking design compared to the monoblock and 2 piece locking designs. This type of comparative simulation between models may reveal important design features that could lead to insight on the success or failure of an implant and improve implant development.

There are several limitations to this study. First, although we selected surrogate bone testing models that are most representative of a nonosteoporotic, nonsclerotic bone, this may not entirely replicate the clinical situation for every patient. The surrogate bone testing model may be less ideal than a cadaveric or clinical model, but efforts were made to simulate the clinical environment, such as using of the epoxy resin sheets with the polyurethane foam blocks

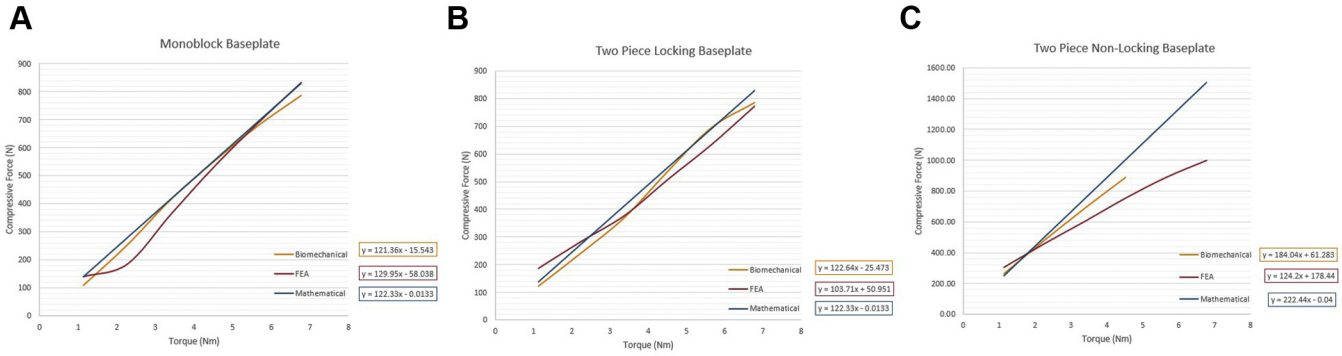

Figure 7 Evaluation of the compression-torque relationship for each baseplate design between predictive models (FEA and mathematical) and biomechanical testing: (**A**) monoblock design, (**B**) 2-piece locking design, and (**C**) 2-piece nonlocking design. *FEA*, finite element analysis.

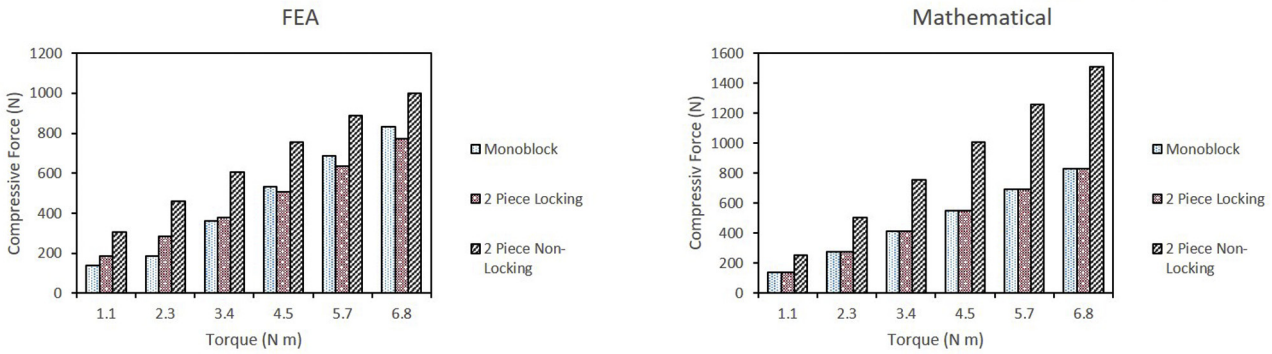

Figure 8 Output of predictive models, FEA and mathematical, illustrating the compressive forces achieved at increasing levels of torque. *FEA*, finite element analysis.

to more closely replicate the glenoid vault. Second, this is a time zero study representing only the initial compression achieved with the central screw of the baseplate within the glenoid vault. No cyclic testing was performed, and peripheral screws were not added to the baseplates. Third, the shape of the backside of the glenoid implant also likely has significant effects on the torque-compression relationship; therefore, the current data may not be generalizable to other RSA baseplate designs, such as those that include a baseplate boss. Fourth, we did not simulate cortical vs. cancellous bone transitions; this may alter the stress and strain distributions on the central screw and minimize the potential for screw strip-out on the cortex of the medial vault. Fifth, in vitro biomechanical, FEA, and mathematical models may not accurately simulate in vivo frictional coefficients between the baseplate-glenoid bone interface as they may be influenced by marrow elements, bleeding in the surgical field, and other aspects not accounted for in the models. The extent to which these affect the torque-compression relationship is unknown. The intrinsic limitation to FEA and mathematical models is that they are deterministic simulations. Although using a probabilistic approach to create a series of simulation allows for statistical interpretation of the data, the computing power and time required to run the appropriate number of simulations can often outweigh the benefits. Moreover, the number of variables to be tested may have to be significantly reduced for the simulations to complete. Additionally, the outcomes of predictive models are highly dependent on the initial assumptions and boundary conditions. Although we maintained our models as close to the biomechanical one, there were conditions we were unable to replicate, such as material strip-out. Lastly, the baseplate designs tested were manufactured out of stainless steel; different material properties of alternative metals may alter the potential failure mechanisms and thresholds.

Conclusion

The torque-compression relationship of a central screw baseplate is significantly affected by baseplate design. A 2-piece non-locking baseplate reaches higher compression levels and risks material strip-out at lower insertional torques compared with a monoblock and locking 2-piece design. This has implications both on component design and on surgeon tactile feedback during surgery.

Disclaimer

This study was funded by DJO Surgical (internal ID: DJO-19-010).

Jason E. Hsu receives royalties and consulting fees from DJO Surgical.

Eric T. Ricchetti receives royalties and consulting fees from DJO Surgical.

Grant E. Garrigues receives consulting payments from DJO Surgical, Wright/Tornier, and Mitek.

Mark A. Frankle receives royalties and consulting fees from DJO Surgical.

The other authors, their immediate families, and any research foundations with which they are affiliated have not received any financial payments or other benefits from any commercial entity related to the subject of this article.

References

1. Ackland DC, Patel M, Knox D. Prosthesis design and placement in reverse total shoulder arthroplasty: review. J Orthop Surg Res 2015;10:101. https://doi.org/10.1186/s13018-015-0244-2.
2. Alentorn-Geli E, Samitier G, Torrens C, Wright TW. Reverse shoulder arthroplasty. Part 2: Systematic review of reoperations, revisions, problems, and complications. Int J Shoulder Surg 2015;9:60–7. https://doi.org/10.4103/0973-6042.154771.
3. Bitzer A, Rojas J, Patten IS, Joseph J, McFarland EG. Incidence and risk factors for aseptic baseplate loosening of reverse total shoulder arthroplasty. J Shoulder Elbow Surg 2018;27:2145–52. https://doi.org/10.1016/j.jse.2018.05.034.
4. Bohsali KI, Bois AJ, Wirth MA. Complications of shoulder arthroplasty. J Bone Joint Surg Am 2017;99:256–69. https://doi.org/10.2106/JBJS.16.00935.
5. Boileau P. Complications and revision of reverse total shoulder arthroplasty. Orthop Traumatol Surg Res 2016;102:S33–43. https://doi.org/10.1016/j.otsr.2015.06.031.
6. Boileau P, Gonzalez JF, Chuinard C, Bicknell R, Walch G. Reverse total shoulder arthroplasty after failed rotator cuff surgery. J Shoulder Elbow Surg 2009;18:600–6. https://doi.org/10.1016/j.jse.2009.03.011.
7. Cameron HU, Pilliar RM, MacNab I. The effect of movement on the bonding of porous metal to bone. J Biomed Mater Res 1973;7:301–11.
8. Chae SW, Kim SY, Lee H, Yon JR, Lee J, Han SH. Effect of baseplate size on primary glenoid stability and impingement-free range of motion in reverse shoulder arthroplasty. BMC Musculoskelet Disord 2014;15:417. https://doi.org/10.1186/1471-2474-15-417.
9. Cheriachan DM, DiPaola M, Iannotti JP, Ricchetti ET. 3D printing in orthopedics—upper extremity arthroplasty. In: DiPaola M, Wodajo FM, editors. 3D printing in orthopaedic surgery. St Louis, MO: Elsevier; 2019. p. 151–69.
10. Cuff DJ, Pupello DR, Santoni BG, Clark RE, Frankle MA. Reverse shoulder arthroplasty for the treatment of rotator cuff deficiency: a concise follow-up, at a minimum of 10 years, of previous reports. J Bone Joint Surg Am 2017;99:1895–9. https://doi.org/10.2106/JBJS.17.00175.
11. Cuff D, Clark R, Pupello D, Frankle M. Reverse shoulder arthroplasty for the treatment of rotator cuff deficiency: a concise follow-up, at a minimum of 5 years, of a previous report. J Bone Joint Surg Am 2012;94:1996–2000. https://doi.org/10.2106/JBJS.K.01206.
12. Dharia MA, Bischoff JE, Schneider D. Impact of modeling assumptions on stability predictions in reverse total shoulder arthroplasty. Front Physiol 2018;9:1116. https://doi.org/10.3389/fphys.2018.01116.
13. Diaz MA, Garrigues GE, Ricchetti ET, Gutierrez S, Frankle MA. The relationship between insertion torque and compression strength in the reverse total shoulder arthroplasty baseplate. J Orthop Res 2020;38:871–9. https://doi.org/10.1002/jor.24506.
14. DiStefano JG, Park AY, Nguten TQ, Diederichs G, Buckley JM, Montgomery WH 3rd. Optimal screw placement for baseplate fixation in reverse total shoulder arthroplasty. J Shoulder Elbow Surg 2011;20:467–76. https://doi.org/10.1016/j.jse.2010.06.001.

15. Inzana JA, Varga P, Windolf M. Implicit modeling of screw threads for efficient finite element analysis of complex bone-implant systems. J Biomech 2016;49:1836–44. https://doi.org/10.1016/j.jbiomech.2016.04.021.
16. Formaini NT, Everding NG, Levy JC, Santoni BG, Nayak AN, Wilson C. Glenoid baseplate fixation using hybrid configurations of locked and unlocked peripheral screws. J Orthop Trauma 2017;18:221–8. https://doi.org/10.1007/s10195-016-0438-3.
17. Formaini NT, Everding NG, Levy JC, Santoni BG, Nayak AN, Wilson C, et al. The effect of glenoid bone loss on reverse shoulder arthroplasty baseplate fixation. J Shoulder Elbow Surg 2015;24:e312–9. https://doi.org/10.1016/j.jse.2015.05.045.
18. Frankle M, Pupello D, Gutierrez S. Rationale and biomechanics of reverse shoulder prosthesis: the American experience. In: Frank MA, editor. Rotator cuff deficiency of the shoulder. New York, NY: Thieme Medical Publishers; 2008. p. 76–104.
19. Frankle M, Siegal S, Pupello D, Saleem A, Mighell M, Vasey M. The reverse shoulder prosthesis for glenohumeral arthritis associated with severe rotator cuff deficiency. A minimum two-year follow-up study of sixty patients. J Bone Joint Surg Am 2005;87:1697–705. https://doi.org/10.2106/JBJS.D.02813.
20. Harman M, Frankle M, Vasey M, Banks S. Initial glenoid component fixation in "reverse" total shoulder arthropplasty: A biomechanical evaluation. J Shoulder Elbow Surg 2005;14(Suppl S):162s–7s. https://doi.org/10.1016/j.jse.2004.09.030.
21. Hopkins AR, Hansen UN, Bull AM, Emery R, Amis AA. Fixation of the reversed shoulder prosthesis. J Shoulder Elbow Surg 2008;17:974–80. https://doi.org/10.1016/j.jse.2008.04.012.
22. Humphrey CS, Kelly JD 2nd, Norris TR. Optimizing glenosphere position and fixation in reverse shoulder arthroplasty, Part two: the three-column concept. J Shoulder Elbow Surg 2008;17:595–601. https://doi.org/10.1016/j.jse.2008.05.038.
23. James J, Huffman KR, Werner FW, Sutton GL, Nanavati VN. Does glenoid baseplate geometry affect its fixation in reverse shoulder arthroplasty? J Shoulder Elbow Surg 2012;21:917–24. https://doi.org/10.1016/j.jse.2011.04.017.
24. Jasty M, Bragdon C, Burke D, O'Connor D, Lowenstein J, Harris WH. In vivo skeletal responses to porous-surfaced implants subjected to small induced motions. J Bone Joint Surg Am 1997;79:707–14.
25. Kang JR, Dubiel MJ, Cofield RH, Steinmann SP, Elhassan BT, Morrey ME, et al. Primary reverse shoulder arthroplasty using contemporary implants is associated with very low reoperation rates. J Shoulder Elbow Surg 2019;28:S175–80. https://doi.org/10.1016/j.jse.2019.01.026.
26. Kempton LB, Ankerson E, Wiater JM. A complication-based learning curve from 200 reverse shoulder arthroplasties. Clin Orthop Relat Res 2011;469:2496–504. https://doi.org/10.1007/s11999-011-1811-4.
27. Kwon YW, Forman RE, Walker PS, Zuckerman JD. Analysis of reverse total shoulder joint forces and glenoid fixation. Bull NYU Hosp Jt Dis 2010;68:273–80.
28. Lawrence C, Williams GR, Namdari S. Influence of glenosphere design on outcomes and complications of reverse arthroplasty: a systematic review. Clin Orthop Surg 2016;8:288–97. https://doi.org/10.4055/cios.2016.8.3.288.
29. Martin EJ, Duquin TR, Ehrensberger MT. Reverse total shoulder glenoid baseplate stability with superior glenoid bone loss. J Shoulder Elbow Surg 2017;26:1748–55. https://doi.org/10.1016/j.jse.2017.04.020.
30. Meisterhans M, Bouaicha S, Meyer DC. Posterior and inferior glenosphere position in reverse total shoulder arthroplasty supports deltoid efficieny for shoulder flexion and elevation. J Shoulder Elbow Surg 2019;28:1515–22. https://doi.org/10.1016/j.jse.2018.12.018.
31. Mole D, Favard L. Excentered scapulohumeral osteoarthritis. Rev Chir Orthop Reparatrice Appar Mot 2007;93:37–94. https://doi.org/10.1016/s0035-1040(07)92708-7 [in French].
32. Nam D, Kepler CK, Neviaser AS, Jones KJ, Wright TM, Craig EV, et al. Reverse total shoulder arthroplasty: current concepts, results, and component wear analysis. J Bone Joint Surg Am 2010;92:23–35. https://doi.org/10.2106/JBJS.J.00769.
33. Oberg E, Jones FD, Horton HL, Ryffel HH, McCauley CJ. Machinery's handbook: a reference book for the mechanical engineer, designer, manufacturing engineer, draftsman, toolmaker and machinist. 29th edition. New York, NY: Industrial Press; 2012. p. 1529–33.
34. Parsons BO, Gruson KI, Accousti KJ, Klug RA, Flatow EL. Optimal rotation and screw positioning for initial glenoshpere baseplate fixation in reverse shoulder arthroplasty. J Shoulder Elbow Surg 2009;18:886–91. https://doi.org/10.1016/j.jse.2008.11.002.
35. Pilliar RM, Lee JM, Maniatopoulos C. Observations on the effect of movement on bone ingrowth into porous-surfaced implants. Clin Orthop Relat Res 1986;208:108–13.
36. Roche CP, Stroud NJ, Flurin PH, Wright TW, Zuckerman JD, DiPaola MJ. Reverse shoulder glenoid baseplate fixation: a comparison of flat-back versus curved-back designs and oval versus circular designs with 2 different offset glenospheres. J Shoulder Elbow Surg 2014;23:1388–94. https://doi.org/10.1016/j.jse.2014.01.050.
37. Somerson JS, Hsu JE, Neradilek MB, Matsen FA 3rd. Analysis of 4063 complications of shoulder arthroplasty reported to the US Food and Drug Administration from 2012 to 2016. J Shoulder Elbow Surg 2018;27:1978–86. https://doi.org/10.1016/j.jse.2018.03.025.
38. Somerson JS, Neradilek MB, Hsu JE, Service BC, Gee AO, Matsen FA 3rd. Is there evidence that the outcomes of primary anatomic and reverse shoulder arthroplasty are getting better? Int Orthop 2017;41:1235–44. https://doi.org/10.1007/s00264-017-3443-0.
39. Stroud NJ, DiPaola MJ, Martin BL, Steiler CA, Flurin PH, Wright TW, et al. Initial glenoid fixation using two different reverse shoulder designs with an equivalent center of rotation in a low-density and high-density bone substitute. J Shoulder Elbow Surg 2013;22:1573–9. https://doi.org/10.1016/j.jse.2013.01.037.
40. Virani NA, Harman M, Li K, Levy J, Pupello DR, Frankle MA. In vitro and finite element analysis of glenoid bone/baseplate interaction in the reverse shoulder design. J Shoulder Elbow Surg 2008;17:509–21. https://doi.org/10.1016/j.jse.2007.11.003.
41. Zhang M, Junaid S, Gregory T, Hansen U, Cheng CK. Effect of baseplate positioning on fixation of reverse total shoulder arthroplasty. Clin Biomech (Bristol, Avon) 2019;62:15–22. https://doi.org/10.1016/j.clinbiomech.2018.12.021.
42. Zumstein MA, Pinedo M, Old J, Boileau P. Problems, complications, reoperations, and revisions in reverse total shoulder arthroplasty: a systematic review. J Shoulder Elbow Surg 2011;20:146–57. https://doi.org/10.1016/j.jse.2010.08.001.